Composite Structures 304 (2023) 116461

Contents lists available at ScienceDirect

Composite Structures

journal homepage: www.elsevier.com/locate/compstruct

Numerical modelling of braided ceramic fiber seals by using element differential method

Yong-Tong Zheng [a,b], Xiao-Wei Gao [b,c,d,*], Yijun Liu [a]

[a] Department of Mechanics and Aerospace Engineering, Southern University of Science and Technology, Shenzhen 518055, China
[b] School of Aeronautics and Astronautics, Dalian University of Technology, Dalian 116024, China
[c] Key Laboratory of Advanced Technology for Aerospace Vehicles of Liaoning Province, Dalian University of Technology, Dalian 116024, China
[d] State Key Laboratory of Structural Analysis for Industrial Equipment, Dalian University of Technology, Dalian 116024, China

ARTICLE INFO

Keywords:
Element Differential Method
Multi-field Interaction Problems
Braided Ceramic Fiber
High Temperature Dynamic Seals
Levenberg-Marquardt Algorithm

ABSTRACT

A new kind of dynamic seal with braided ceramic fibers has been designed to seal the movable panels in the scramjet engines, which are used for the propulsion of hypersonic vehicle. The braided ceramic fiber structure can provide buffer forces when the seals are subjected to the external dynamical preloads. However, it also makes the seals difficult to analyze. Up to now, the analysis of the seals still uses 1D models so that one cannot implement the coupled analysis of seals and their surrounding structures and flows. In this paper, a novel 2D and 3D mechanics-thermal-seepage coupled model is proposed to describe these seals, which provides a possibility for the aforementioned coupled analysis. Meanwhile, a strong-form numerical method, element differential method (EDM) is employed to discretize the governing equations of the coupled model due to its efficiency and robustness. Three examples are given. The first one is to invert the material-dependent parameters of three kinds of seal strips from the experimental data by Levenberg-Marquardt (LM) algorithm. Other two implement the analyses of 3D square and circular cross-section seals, respectively, which verify that EDM is more efficient than FEM in seal analysis when using the same mesh sizes.

1. Introduction

1.1. High temperature braided rope dynamic seals

Hypersonic vehicles (that is, aircraft whose speed can exceed 5 Ma) have become hot research fields in many countries and areas. As a kind of hypersonic vehicle engines, scramjet engines can provide enough traction needed, for which the conventional turbojet engines cannot. However, scramjet engines cannot launch by themselves at low speed. A turbine based combined cycle (TBCC) technology can solve this problem [1–4]. In order to make the TBCC adjustable inlet work normally, certain gaps must be reserved between the adjustable board and outside shell when the engine is working. At low speed, the effect of the gaps is relatively small and can be ignored. However, in the supersonic flight, the high-speed air will flow into the gap, which will produce extremely high temperature at the gaps. Then, the gaps may be expanded due to ablation, which may cause some unexpected changes and lead to an accident in flight finally. To avoid this, the gaps must be sealed dynamically. Usually, scramjet engines need to work in the higher temperature and worse environment than the conventional turbojet engines. Therefore, the dynamic seals, which are used to prevent the high temperature gases from being leaked, should bear higher thermal loads, higher pressure difference, and larger deformations than the seals used on turbojet engines [5–10].

Although the working environment is harsh, a kind of dynamic seal is still designed to cater to the need of the scramjet engines. As shown in Fig. 1, the seal strips use core-sheath architecture. The core and sheath are both made of a lot of braided ceramic fibers. Sheath has a certain braided angle to protect core from falling apart, while core occupies almost 90 % volumes of the whole seal strip structure [9]. Generally, the seals have a porosity of 0.5–0.6 without any external force acting. In the practical applications, the seal is subjected to a transverse preload so that the porosity will be decreased with deformation, which restrict the leakage flow from going through the seal transversely. Fig. 2 shows a 3D working illustration of a seal system. Actually, in addition to circular cross-sections as shown in Fig. 1, square cross-sections are also common for this type of seal, as shown in Fig. 3(a).

Analyzing these dynamic seals numerically is the prerequisite of

* Corresponding author.
E-mail address: xwgao@dlut.edu.cn (X.-W. Gao).

https://doi.org/10.1016/j.compstruct.2022.116461
Received 31 August 2022; Received in revised form 23 October 2022; Accepted 6 November 2022
Available online 9 November 2022

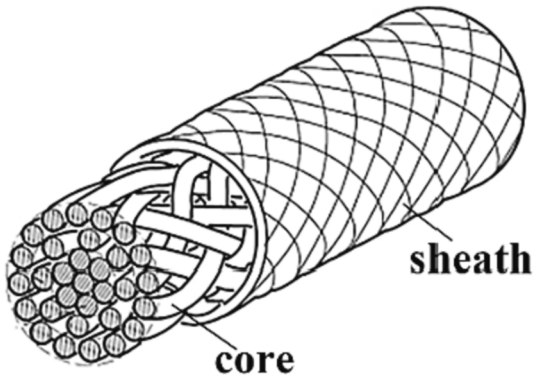

Fig. 1. Core-sheath architecture of the circular cross-section seal strip [5].

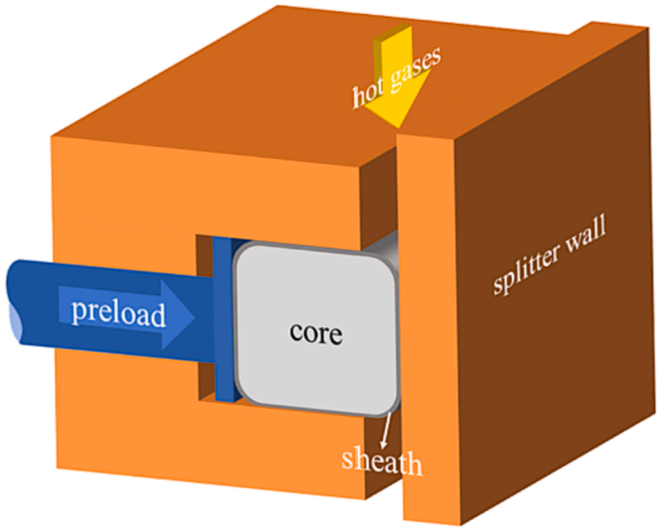

Fig. 2. Working illustration of the seal system [9,10].

realizing the coupled analysis of the seals with their surrounding structures and fluid. However, plenty of braided fibers make the strictly precise analysis scarcely possible. So, some researchers considered the seal strip as a whole entity to reveal the physics regulation of some significant indicator of the seal strip, for example, leakage rate. Mutharasan, Steinetz and Cai et al [6–10] explored the relationships between the leakage rate and some possible factors that may affect it by experimental results and theoretical analysis. Mutharasan [8] established a 1D mathematical model of the seal strips based on the Kozeny-Carman equation. The model reveals that the leakage rate is affected by porosity, gas properties, fiber diameter, and gas pressure difference across the seal etc. Based on Mutharasan's work, Cai et al [10] proposed a modified model that take the preload into account by assuming the relationships among leakage resistance, preload, and pressure difference across the seal. Meanwhile, they [9] also found that the modified Ergun equation [11] is more reasonable and more accurate to describe the leakage flow than the original Kozeny-Carman equation.

Only 1D models are considered in the aforementioned research works. In 1D models, the leakage resistance is derived by integrating 1D Kozeny-Carman equation directly [7–10], which is just like a bridge to associate the leakage rate with the seal properties, gas properties, preload, and pressure difference. Some parameters of seal samples are obtained by using least squares linear regression method to fit the experimental results [9,10]. However, it is quite simple to describe the working processes of the seals and cannot be used in coupled analysis with surrounding structures and fluids. In this paper, a multi-dimensional (2D and 3D) mechanics-thermal-seepage coupled model is proposed not only to predict the leakage rate of the seal strips, but also to provide the distribution of temperatures, seepage pressures and displacements in the seals.

1.2. Element differential method

When establishing a multi-dimensional model, ordinary differential equations (ODEs) turn into partial differential equations (PDEs). Therefore, leakage resistance is not applicable anymore because one cannot obtain an explicit equation by directly integrating a complex PDE. In practical engineering, numerical methods are the most commonly used tools to deal with the complex PDEs, which include finite element method (FEM) [12], boundary element method (BEM) [13], mesh reduction method (MRM) [14] etc. In solid mechanics, FEM occupies a dominant position. Especially, in recent years, newly proposed isogeometric FEM analysis fills the gap between computer-aided design (CAD) and FEM [15,16]. In this paper, another recently proposed numerical method, element differential method (EDM) [17–27], is employed to solve this multi-field interaction problem. EDM is firstly proposed by Gao et al [18,26], and applied to solve heat conduction problems and thermal-mechanics problems. EDM belongs to the categories of collocation method and FEM in a broad sense. It can obtain more stable solutions than some other collocation methods due to the use of element mapping technique and it is more efficient than traditional Galerkin FEM due to its sparser coefficient matrix. Up to now, EDM has been applied to analyze solid vibration problems [24], piezoelectric problems [21], electromagnetic wave problems [22] etc. In this paper, EDM will be applied to analyze this multi-field interaction nonlinear problem for the first time. Also, it is the first time to deal with the time derivative term of volumetric and anisotropic constitutive by using EDM.

Besides, to complete the proposed mechanics-thermal-seepage coupled model, the authors specify the functional expressions of some material properties, which contain the material-dependent parameters and the physical quantities to be solved. Therefore, the resulted set of algebraic equations is non-linear and will be solved by Newton iterative method. Three examples are given in this paper. In the first example, Levenberg-Marquardt (LM) algorithm [28–31] is employed to invert

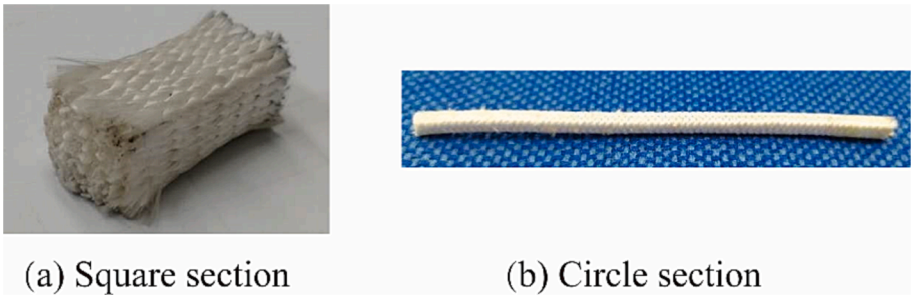

Fig. 3. Photograph of square cross-section seal and circle cross-section seal.

material-dependent parameters of three kinds of seal strips from the experimental results. The second and third examples use the proposed 3D model to analyze the square and circular cross-section seal strips, respectively. The results and the efficiency of two numerical methods, EDM and conventional Galerkin FEM, for computing these problems will be compared.

2. Governing equations of seepage, deformation and heat conduction as well as the relationships among some essential parameters

To analyze the physical processes of the braided ceramic seal strips, a mathematical model should be set up first. Obviously, it is extremely complicated to consider the squeezing and friction between any two fibers and the interactions between fibers and fluid in detail. Therefore, in this section, a mechanics-thermal-seepage coupled model is proposed instead of the complicated analysis above [32].

2.1. Governing equations of seepage

The seal strips can be regarded as the porous media and the process of fluid going through porous media can be described by the seepage equation, i.e., [33,34].

$$\frac{\rho_l}{\rho_0}\frac{\partial \varepsilon_v}{\partial t}+\Phi\beta_p\frac{\partial P}{\partial t}+\Phi\beta_t\frac{\partial T}{\partial t} = \frac{\partial}{\partial x_i}\left(\frac{\alpha}{\upsilon}\frac{\partial P}{\partial x_i}\right) \tag{1}$$

where x_i is the coordinate of i-th direction (coordinate (x, y, z)= (x_1, x_2, x_3) in this paper); P is the seepage pressure; T is the temperature; t is time; α is permeability; υ is dynamic viscosity coefficient of fluid; ε_v is volumetric strain; Φ is porosity; β_p is compressibility coefficient of fluid; β_t is the thermal volume expansion coefficient of fluid; ρ_l/ρ_0 represents the ratio of local fluid density ρ_l and reference fluid density ρ_0 (equals 1.178 kg/m^3 in this paper) and can be computed by [33,34].

$$\frac{\rho_l}{\rho_0} = \frac{P\cdot T_0}{P_0\cdot T} \tag{2}$$

where T_0 and P_0 are the reference temperature and seepage pressure when the seal has no deformation (equal 300 K and 1 atm in this paper). In this paper, repeated subscripts represent summation and they can be 1 or 2 for 2D problems, be 1, 2, or 3 for 3D problems, respectively. There are two kinds of boundary conditions for the seepage equation:

$$P = \overline{P} \tag{3}$$

$$-\frac{\alpha}{\upsilon}\frac{\partial P}{\partial x_i}\cdot n_i = \overline{v} \tag{4}$$

where $\overline{P}$ and $\overline{v}$ are the prescribed seepage pressure and velocity, respectively; n_i is the i-th direction of outer normal vector.

2.2. Governing equations of mechanics

The deformation of seals subjected to preloads can be described as elasticity equations without the body force term [33,34]:

$$\frac{\partial \sigma_{ij}}{\partial x_j} = 0 \tag{5}$$

$$\sigma_{ij} = C_{ijkl}\varepsilon_{kl} - \kappa_{ij}(T - T_0) - b\delta_{ij}(P - P_0) \tag{6}$$

$$\varepsilon_{ij} = \frac{1}{2}\left(\frac{\partial u_i}{\partial x_j}+\frac{\partial u_j}{\partial x_i}\right) - \beta\delta_{ij}(T - T_0) \tag{7}$$

in which σ_{ij} represents stress tensor; C is the elastic constitutive tensor; ε_{ij} is strain tensor; u_i is the displacement of the i-th direction; δ_{ij} is Kronecker Delta; b is Biot coefficient, which characterize the effect of seepage pressure on stress; β is thermal expansion coefficient; κ_{ij} is thermal stress tensor. Usually, two kinds of boundary conditions of elasticity are used:

$$u_i = \overline{u_i} \tag{8}$$

$$\sigma_{ij}\cdot n_j = \overline{t_i} \tag{9}$$

where $\overline{u_i}$ and $\overline{t_i}$ are the prescribed displacement and surface traction, respectively.

In Eq., elastic constitutive tensor C is a fourth order tensor. In general, because the seal strip is made of braided fibers, the mechanics properties along the length orientation are different from the other two radial orientations. However, for 2D problems, only a section of seal strip is considered, so that 2D problems can be regarded as isotropic problems. For isotropic problem, elastic constitutive tensor C can be expressed by formula.

$$C_{ijkl} = \lambda\delta_{ij}\delta_{kl} + \mu\left(\delta_{ik}\delta_{jl} + \delta_{il}\delta_{jk}\right) \tag{10}$$

in which λ and μ are Lamé constants and they can be expressed by formula.

$$\lambda = \frac{E\nu}{(1+\nu)(1-2\nu)} \tag{11}$$

$$\mu = \frac{E}{2(1+\nu)} \tag{12}$$

where E and ν are the equivalent elastic modulus and Poisson ratio of the material, respectively. Due to the symmetry of shear stress and shear strain, fourth order tensor C, which has 16 elements, can be simplified into 9 elements. Meanwhile, Eq.(6) can be simplified as the following 3 × 3 matrix format for 2D problems.

$$\begin{bmatrix}\sigma_{11}\\ \sigma_{22}\\ \sigma_{12}\end{bmatrix} = \begin{bmatrix}\lambda+2\mu & \lambda & 0\\ \lambda & \lambda+2\mu & 0\\ 0 & 0 & \mu\end{bmatrix}\begin{bmatrix}\varepsilon_{11}\\ \varepsilon_{22}\\ \varepsilon_{12}\end{bmatrix} \tag{13}$$

But for 3D problems, the effect of anisotropy must be considered. This kind of anisotropy can be regarded as orthotropic anisotropy and requires nine independent parameters to determine the constitutive tensor C, which are elastic moduli of three orientations E_1, E_2 and E_3, three main Poisson ratios ν_{12}, ν_{13} and ν_{23} and three shear moduli G_{12}, G_{13} and G_{23}. Besides, there are three deputy Poisson ratios ν_{21}, ν_{31} and ν_{32}, which can be calculated by three main Poisson ratios and three elastic moduli, i.e.,

$$\begin{cases}\frac{\nu_{12}}{E_1} = \frac{\nu_{21}}{E_2}\\ \frac{\nu_{13}}{E_1} = \frac{\nu_{31}}{E_3}\\ \frac{\nu_{23}}{E_2} = \frac{\nu_{32}}{E_3}\end{cases} \tag{14}$$

Similar to 2D problems, Eq. can also be simplified as the following 6 × 6 matrix format.

$$\begin{bmatrix}\sigma_{11}\\ \sigma_{22}\\ \sigma_{33}\\ \sigma_{12}\\ \sigma_{13}\\ \sigma_{23}\end{bmatrix} = \begin{bmatrix}CM_{11} & CM_{12} & CM_{13} & 0 & 0 & 0\\ CM_{21} & CM_{22} & CM_{23} & 0 & 0 & 0\\ CM_{31} & CM_{32} & CM_{33} & 0 & 0 & 0\\ 0 & 0 & 0 & CM_{44} & 0 & 0\\ 0 & 0 & 0 & 0 & CM_{55} & 0\\ 0 & 0 & 0 & 0 & 0 & CM_{66}\end{bmatrix}\begin{bmatrix}\varepsilon_{11}\\ \varepsilon_{22}\\ \varepsilon_{33}\\ \varepsilon_{12}\\ \varepsilon_{13}\\ \varepsilon_{23}\end{bmatrix} \tag{15}$$

in which.

$$CM_{11} = \frac{1-\nu_{23}\nu_{32}}{E_2E_3\Delta} \tag{16}$$

$$CM_{12} = CM_{21} = \frac{\nu_{21}+\nu_{31}\nu_{23}}{E_2E_3\Delta} = \frac{\nu_{12}+\nu_{13}\nu_{32}}{E_1E_3\Delta} \tag{17}$$

$$CM_{22} = \frac{1-\nu_{13}\nu_{31}}{E_1E_3\Delta} \tag{18}$$

$$CM_{23} = CM_{32} = \frac{\nu_{32} + \nu_{12}\nu_{31}}{E_1E_3\Delta} = \frac{\nu_{23} + \nu_{21}\nu_{13}}{E_1E_2\Delta} \tag{19}$$

$$CM_{33} = \frac{1-\nu_{12}\nu_{21}}{E_1E_2\Delta} \tag{20}$$

$$CM_{13} = CM_{31} = \frac{\nu_{13} + \nu_{12}\nu_{23}}{E_1E_2\Delta} = \frac{\nu_{31} + \nu_{21}\nu_{32}}{E_2E_3\Delta} \tag{21}$$

$$CM_{44} = G_{12} \tag{22}$$

$$CM_{55} = G_{13} \tag{23}$$

$$CM_{66} = G_{23} \tag{24}$$

where.

$$\Delta = \frac{1}{E_1E_2E_3}\begin{vmatrix} 1 & -\nu_{21} & -\nu_{31} \\ -\nu_{12} & 1 & -\nu_{32} \\ -\nu_{13} & -\nu_{23} & 1 \end{vmatrix} \tag{25}$$

Furthermore, because the mechanics properties of two radial orientations of seal strip can be regarded the same, 9 independent parameters can be reduced to 5. Supposing the length orientation is along axis x_1, the following 4 formulas are satisfied.

$$\begin{cases} E_2 = E_3 \\ \nu_{12} = \nu_{13} \\ G_{12} = G_{13} \\ G_{23} = \dfrac{1-\nu_{13}\nu_{31}-\nu_{32}-\nu_{12}\nu_{31}}{2E_1E_3\Delta} \end{cases} \tag{26}$$

Thus, 9 parameters can be reduced to 5, i.e., elastic moduli of two orientations E_1 and E_2, two main Poisson ratios ν_{12} and ν_{23}, and shear moduli G_{12}.

For either 2D or 3D problems, the thermal stress tensor κ_{ij} can be expressed by a unified formula.

$$\kappa_{ij} = \begin{cases} C_{ijkk}\beta \ i = j \\ 0 \ i \neq j \end{cases} \tag{27}$$

Specifically, for 2D isotropic problems,

$$\kappa_{11} = \kappa_{22} = 2(\lambda+\mu)\beta \tag{28}$$

and for 3D anisotropic problems,

$$\begin{cases} \kappa_{11} = (CM_{11} + CM_{12} + CM_{13})\beta \\ \kappa_{22} = \kappa_{33} = (CM_{21} + CM_{22} + CM_{23})\beta \end{cases} \tag{29}$$

2.3. Governing equations of heat conduction

The equation that describes the heat transfer process is [33,34].

$$\rho c_p \frac{\partial T}{\partial t} + (1-\Phi)\kappa_{jk}T_0\frac{\partial \varepsilon_{jk}}{\partial t} = \frac{\partial}{\partial x_i}\left(K\frac{\partial T}{\partial x_i}\right) \tag{30}$$

where K is equivalent thermal conductivity; $\rho \cdot c_p$ is equivalent density multiplying specific heat. The word 'equivalent' means that the relevant properties are mixed by those of fluid and fibers according to porosity, i.e.,

$$K = (1-\Phi)K_s + \Phi K_l \tag{31}$$

$$\rho c_p = (1-\Phi)\rho_s c_{ps} + \Phi\rho_l c_{pl} \tag{32}$$

in which subscript s represents solid and l represents fluid. Two kinds of boundary conditions of heat conduction equation are expressed as follows.

$$T = \overline{T} \tag{33}$$

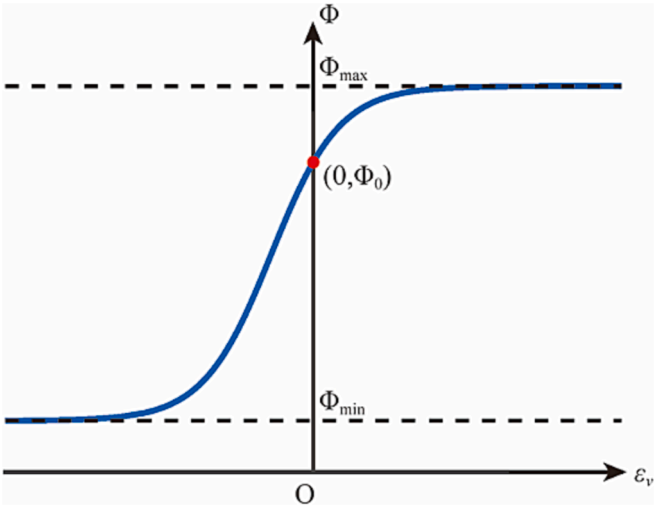

Fig. 4. Schematic show of porosity and volumetric strain.

$$-K\cdot\frac{\partial T}{\partial x_i}\cdot n_i = \overline{q} \tag{34}$$

where $\overline{T}$ and $\overline{q}$ are the prescribed temperature and heat flux, respectively.

2.4. Evolution relationships between parameters

Porosity is an important parameter of the porous media. For seal strips, the porosity is affected mainly by the volumetric strain ε_v. It can be found from the previous experiments [10] that porosity changes under different preloads and seepage pressures. This is because preloads and seepage pressures both affect the strain tensor. To obtain the exact relationship between porosity and volumetric strain, generally, the porosity should be experimentally measured under different working conditions. With no preload and seepage pressure, the seal strip porosity is approximately homogeneous and can be easily measured [9,10]. However, it is not homogeneous and cannot be easily measured when the seal strip is deformed. Therefore, in this paper, an empirical equation is proposed in the following to describe the relationship between the seal strip porosity and volumetric strain:

$$\frac{1}{\Phi-\Phi_{\min}} - \frac{1}{\Phi_{\max}-\Phi_{\min}} = \left(\frac{1}{\Phi_0-\Phi_{\min}} - \frac{1}{\Phi_{\max}-\Phi_{\min}}\right)\cdot\exp(-a\varepsilon_v) \tag{35}$$

in which $\Phi_{\min}$, $\Phi_{\max}$, and Φ_0 represent the minimum porosity, maximum porosity, and the porosity without deformation; a is an evolution parameter which must be greater than 0. Fig. 4 visualizes their basic relationship. Through Fig. 4, it can be found that porosity changes fast near $\varepsilon_v = 0$ and have little variation when it comes to $\Phi_{\min}$ and $\Phi_{\max}$. The change of parameter a mainly affects the slope of the curve near $\varepsilon_v = 0$. By referencing to [10], in this paper, $\Phi_{\min}$ and $\Phi_{\max}$ are set as 0.093 and 0.7, respectively. As for Φ_0, different kind of seal strips have different values.

Meanwhile, the porosity affects the permeability. In this paper, the relational expression about porosity and permeability is adopted from reference [9], i.e.,

$$\alpha = \alpha_0\frac{\Phi^2}{(1-\Phi)^3} \tag{36}$$

in which α_0 is an experimental parameter and is also greater than 0. The equivalent elastic modulus of the seal strip is related to the porosity and temperature, which can be expressed as.

$$E = E_0(1-\Phi)(1-a_1\ (T-T_0)\ ) \tag{37}$$

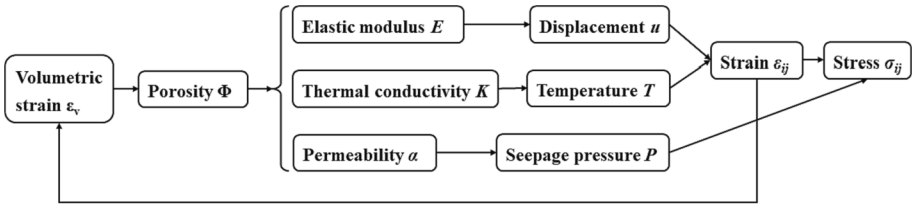

Fig. 5. The illustration of relationships among physical quantities.

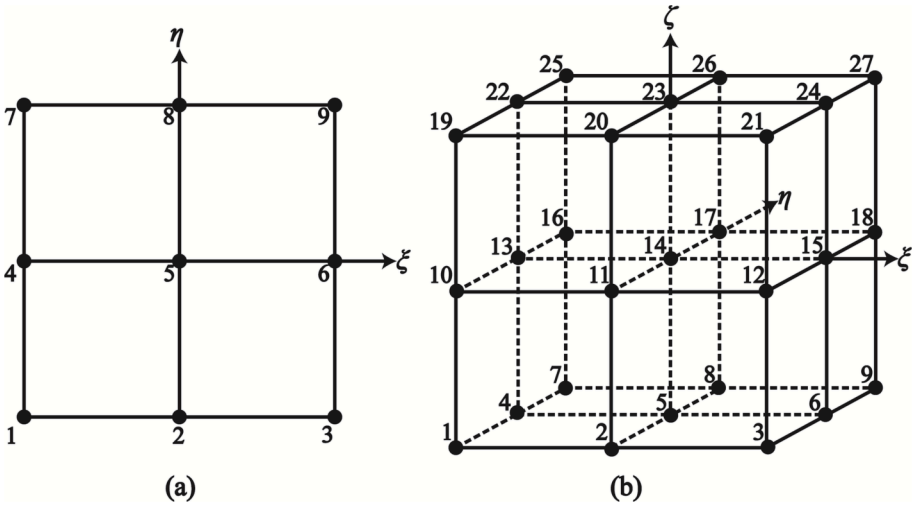

Fig. 6. 2D 9-node and 3D 27-node Lagrange elements.

where E_0 is also an experimental parameter, the value of which is much smaller than that of the transverse elastic modulus of ceramic fibers; a_1 is a parameter that characterizes how much temperature affects elastic modulus.

Thus, the complicated working process of the seal strip is simplified as a non-linear multi-field interaction problem. The relationships among the physical quantities are illustrated in Fig. 5.

3. Discretization of the non-linear PDEs by using EDM

In this paper, the element differential method (EDM) [12–21]is used to discretize the partial differential equations (PDEs) into several algebraic equations and the Newton method is used to solve the non-linear algebraic equation set.

3.1. Theory of EDM

Element differential method is a strong-form numerical method. Like conventional FEM, it can use various isoparametric elements to discretize the computational domains. In this paper, the 2D 9-node and 3D 27-node Lagrange elements are used, as shown in Fig. 6. Physical variable u and coordinate x_i over these elements can be expressed as linear combinations of variable u and coordinate x_i at all nodes, i.e.

$$u = N_\alpha u^\alpha \tag{38}$$

$$x_i = N_\alpha x_i^\alpha \tag{39}$$

where N_α is the shape function of node α. Similarly, the first and the second order derivatives of physical variable u can also be expressed as.

$$\frac{\partial u}{\partial x_i} = \frac{\partial N_\alpha}{\partial x_i} u^\alpha \tag{40}$$

$$\frac{\partial^2 u}{\partial x_i \partial x_j} = \frac{\partial^2 N_\alpha}{\partial x_i \partial x_j} u^\alpha \tag{41}$$

The detailed formula of shape functions and its first or second order derivatives can be found in references [18,26] and would not be shown here.

EDM is a collocation method and it obeys the rule that different kinds of nodes use different equations. There are two kinds of nodes in EDM, element internal nodes and element boundary nodes. For 2D 9-node Lagrange element shown in Fig. 6 (a), node 5 is the element internal node. For 3D 27-node Lagrange element shown in Fig. 6 (b), node 14 is the element internal node. The other nodes of 9-node and 27-node elements are the element boundary nodes.

For element internal nodes, directly discretized governing equations are used. Here, the governing Eqs., and without the time items (steady state equations) are considered first. By substituting Eqs. and into the governing equations, they can be expressed as.

$$\left[\frac{\partial N_\beta}{\partial x_j} C_{ijkl}^\beta \frac{\partial N_\alpha}{\partial x_l} + C_{ijkl} \frac{\partial^2 N_\alpha}{\partial x_i \partial x_j}\right] u_k^\alpha - \frac{\partial N_\alpha}{\partial x_j}\left(\kappa_{ij}(T - T_0)\right)^\alpha - \frac{\partial N_\alpha}{\partial x_i}\left(b(P - P_0)\right)^\alpha = 0 \tag{42}$$

$$\left[\frac{\partial N_\beta}{\partial x_i} K^\beta \frac{\partial N_\alpha}{\partial x_i} + K \frac{\partial^2 N_\alpha}{\partial x_i \partial x_i}\right] T^\alpha = 0 \tag{43}$$

$$\left[\frac{\partial N_\beta}{\partial x_i} \frac{\alpha^\beta}{\upsilon} \frac{\partial N_\alpha}{\partial x_i} + \frac{\alpha}{\upsilon} \frac{\partial^2 N_\alpha}{\partial x_i^2}\right] P^\alpha = 0 \tag{44}$$

In this paper, direct integration method is applied to deal with the time items. If substituting G_n and H_n for the left side of Eqs.(43) and (44) at n-th time step, respectively, element internal node equations with the time items can be expressed as.

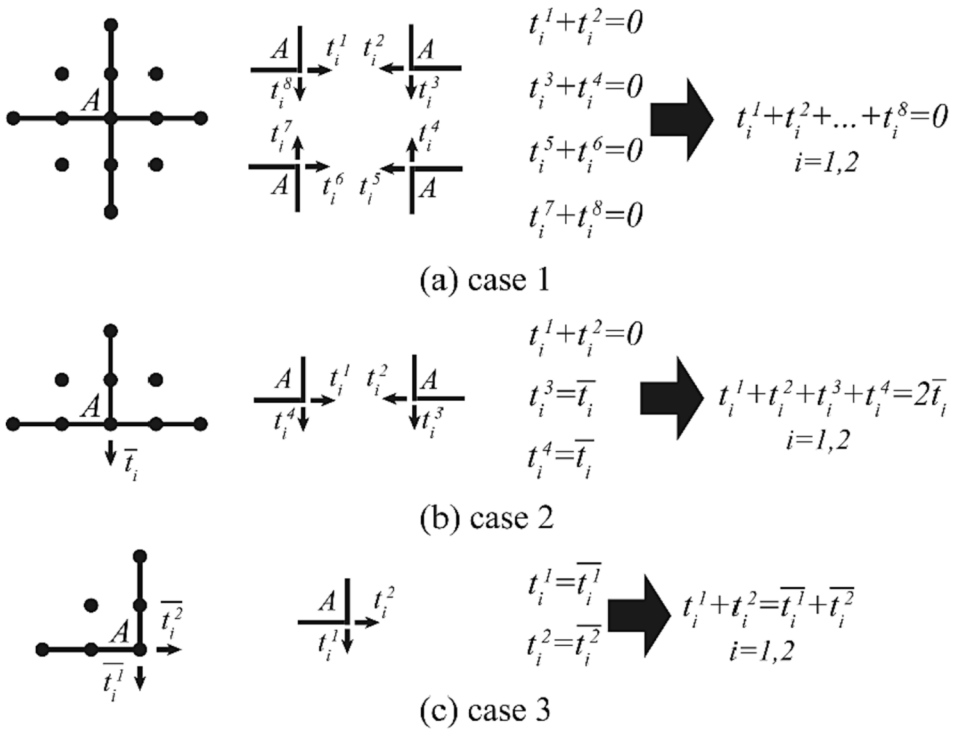

Fig. 7. Three kinds of common cases of element boundary nodes [19].

$$\rho c_p \frac{T_{n+1}-T_n}{\Delta t}+(1-\Phi)\kappa_{jk}T_0\frac{\partial N_\alpha}{\partial x_k}\frac{\left(u_j^\alpha\right)_{n+1}-\left(u_j^\alpha\right)_n}{\Delta t} = \theta G_{n+1}+(1-\theta)G_n \tag{45}$$

$$\frac{\rho_l}{\rho_0}\frac{\partial N_\alpha}{\partial x_i}\frac{\left(u_i^\alpha\right)_{n+1}-\left(u_i^\alpha\right)_n}{\Delta t}+\Phi\beta_p\frac{P_{n+1}-P_n}{\Delta t}+\Phi\beta_t\frac{T_{n+1}-T_n}{\Delta t} = \theta H_{n+1}+(1-\theta)H_n \tag{46}$$

where Δt is the length of time step; subscript n or $n+1$ represent that the variables belong to n-th or $(n+1)$-th step; θ satisfies $0<\theta\leqslant 1$ [17] and equals 1 in the examples below.

The equations for element boundary nodes are the surface traction, heat flux, or velocity equilibrium equations, i.e.,

$$\sum_{e=1}^{N}\left[\left(C_{ijkl}\frac{\partial N_\alpha}{\partial x_l}u_k^\alpha-\kappa_{ij}(T-T_0)-b\delta_{ij}(P-P_0)\right)\sum_{f=1}^{M}n_j^f\right]=\sum_{e=1}^{N}\sum_{f=1}^{M}\overline{t_i^f}\text{ or }0 \tag{47}$$

$$-\sum_{e=1}^{N}\left[\left(K\frac{\partial N_\alpha}{\partial x_i}T^\alpha\right)\sum_{f=1}^{M}n_i^f\right]=\sum_{e=1}^{N}\sum_{f=1}^{M}\overline{q^f}\text{ or }0 \tag{48}$$

$$-\sum_{e=1}^{N}\left[\left(\frac{\alpha}{\upsilon}\frac{\partial N_\alpha}{\partial x_i}P^\alpha\right)\sum_{f=1}^{M}n_i^f\right]=\sum_{e=1}^{N}\sum_{f=1}^{M}\overline{v^f}\text{ or }0 \tag{49}$$

in which N is the number of elements related to the collocation node; M is the number of surfaces in element e which this node is located on; e and f are the element number and surface number, respectively. Generally, if the node is located on the boundary of the whole model, the right-hand sides of three equations may not be zero. However, if the node is not located on the boundary, the right-hand sides must be zero. To illustrate equilibrium equations in detail, three common cases of element boundary nodes are shown in Fig. 7, where t in the figure represents the surface traction. Of course, when the mesh is distorted, there are many other complicated cases which are not discussed here.

Based on the discretized equations above, each node has two or three (being the number of dimensions) deformation equations, one thermal equation, and one seepage equation, four or five equations in total for 2D or 3D, respectively. For each time step, a non-linear equation set can be formed by collecting these equations together. Writing it into a matrix and vector form, it follows that.

$$[A(x_n,x_{n+1})]\{x_{n+1}\}=\{b(x_n)\} \tag{50}$$

in which $[A]$ is the coefficient matrix; $\{x_n\}$ and $\{x_{n+1}\}$ are the solution vector of n-th and $(n+1)$-th steps, respectively; $\{b\}$ is the right-hand side vector. If the initial solution vector is specified, the solution vector of each step can be computed from the previous step. Usually, the Newton iterative method is used to solve the non-linear equation set at each step.

3.2. Newton iterative method

Newton iterative method can transform the process of solving a system of non-linear algebraic equations, such as Eq., into solving a system of linear algebraic equations several times. Supposing that $\{x_n\}$ is the guess vector of n-th step, then, residual vector $\{R\}$ is defined as.

$$\{R\}=\{b\}-[A(x_n)]\{x_n\} \tag{51}$$

Then, the next guess vector $\{x_{n+1}\}$ can be computed by formula.

$$\{x_{n+1}\}=\{x_n\}+w\cdot A^{-1}(x_n)\cdot\{R\} \tag{52}$$

where w is relaxation factor taking value between 0.7 ~ 1.0 and is set to 1.0 in this paper. When the ∞-norm of the residual vector is less than a certain limit (usually 10^{-4}), $\{x_{n+1}\}$ can be regarded as the final solution of this non-linear equation set.

4. Example 1: Determination of a, α_0, and E_0 from the experiments by an inverse procedure

In this example, the parameters a, α_0, and E_0 are determined through an inverse procedure from the experimental results mentioned in reference [10], which contain 26 groups of leakage rates of each seal

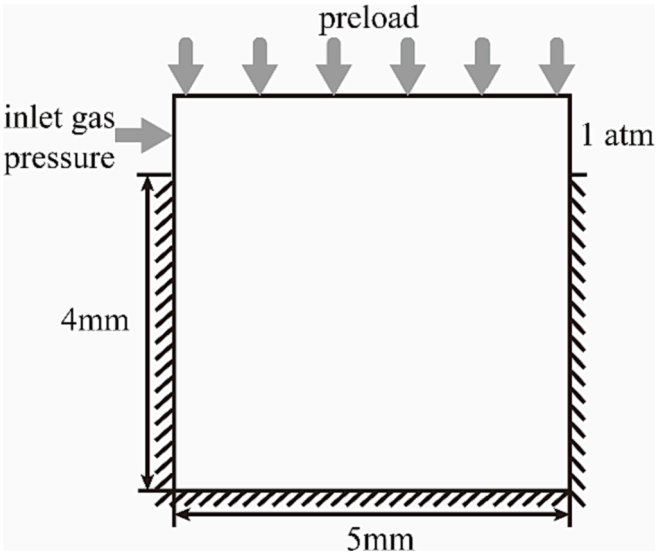

Fig. 8. The computational model of the example 1.

under different preloads, different inlet gas pressures. The experimental data are all measured under normal temperature (about 300 K) at steady state. Therefore, the heat transfer equation (include parameter a_1) and time items in all equations can be ignored in this example.

4.1. Levenberg-Marquardt (LM) algorithm

Inverting three unknown parameters mentioned above can be regarded as a problem of minimizing the following objective function:

$$F(a,\alpha_0,E_0)=\sqrt{\frac{1}{M}\sum_{i=1}^{M}\left(\overline{L_i}-L_i(a,\alpha_0,E_0)\right)^2} \tag{56}$$

where M is the group number of measured leakage rates under different preloads and seepage pressures in the experiments; $\overline{L_i}$ is the experimental value of the i-th leakage rate, while L_i is the computational value of it.

LM algorithm is a gradient iterative algorithm that can find the minimum value of the objective function. In n-th iterative step, the vector that consists of three parameters is updated by the following formula.

$$\begin{Bmatrix} a \\ \alpha_0 \\ E_0 \end{Bmatrix}_{n+1}=\begin{Bmatrix} a \\ \alpha_0 \\ E_0 \end{Bmatrix}_{n}+\begin{Bmatrix} \delta a \\ \delta\alpha_0 \\ \delta E_0 \end{Bmatrix} \tag{57}$$

where the front δ means the increment of the parameter in this step and the increment vector can be computed by formula.

$$\left([J]^T[J]+c\cdot diag\left([J]^T[J]\right)\right)\begin{Bmatrix} \delta a \\ \delta\alpha_0 \\ \delta E_0 \end{Bmatrix}=[J]^T\{D\} \tag{58}$$

in which $[J]$ is sensitivity coefficient matrix; c is the damping factor (equals 0.001 in this example); *diag* means only the diagonal elements of a matrix are remained and the other elements are set to zero; $\{D\}$ is a vector of M elements and can be expressed as.

$$\{D\}=\begin{Bmatrix} \overline{L_1}-L_1(a,\alpha_0,E_0) \\ \overline{L_2}-L_2(a,\alpha_0,E_0) \\ \cdots\cdots \\ \overline{L_M}-L_M(a,\alpha_0,E_0) \end{Bmatrix} \tag{59}$$

And $[J]$ is an $M\times 3$ matrix, which can be expressed as.

Table 1
Parameters a, α_0, E_0 for three different seal strips that minimize F.

	a	α_0	E_0
M6a-1	1.905695	6.333553×10^{-12}	8.585619×10^{6}
M6b-1	1.957233	5.505652×10^{-12}	1.093146×10^{7}
M6c-1	1.955108	7.994810×10^{-12}	9.868145×10^{6}

$$[J]=\begin{bmatrix} \frac{\partial L_1}{\partial a} & \frac{\partial L_1}{\partial \alpha_0} & \frac{\partial L_1}{\partial E_0} \\ \frac{\partial L_2}{\partial a} & \frac{\partial L_2}{\partial \alpha_0} & \frac{\partial L_2}{\partial E_0} \\ \cdots & \cdots & \cdots \\ \frac{\partial L_M}{\partial a} & \frac{\partial L_M}{\partial \alpha_0} & \frac{\partial L_M}{\partial E_0} \end{bmatrix} \tag{60}$$

In this paper, the derivatives in matrix $[J]$ is computed by differences, such as the following formula.

$$\frac{\partial L_i(a,\alpha_0,E_0)}{\partial a}=\frac{L_i(1.01a,\alpha_0,E_0)-L_i(a,\alpha_0,E_0)}{0.01a} \tag{61}$$

The iteration is terminated until the objective function F is within a specified tolerance (10^{-4} in this example) compared with the previous step.

4.2. Computation and analysis

To compute the leakage rates by using EDM, a computational model should be set up. If considering the cross section far away from two sides of seal strip, the model can be regarded as plane strain state. In this example, the cross section of the seal strip is square. Fig. 8 shows the model of the seal strip. Top right of the square is exposed to 1 atm (101325 Pa) pressure, while top left is exposed to different gas pressure (greater than1 atm). The other boundaries have no gas leakage, which means the flow velocities are 0. The upper boundary is subjected to uniform preload. Lower left, lower right and bottom of the square are fixed. 2500 (50 × 50) 9-node elements are used to discretize the computational model and there are 10,201 nodes in total.

There are some other material parameters should be specified. Poisson ratio is set to 0.22. Dynamic viscosity coefficient of the air is 1.79×10^{-5} Pa·s. Biot coefficient is set to 1.0. Then, if specifying three material-dependent parameters a, α_0, E_0, and initial porosity Φ_0, the seepage pressures and displacements of the whole computational domain can be computed by EDM. Then, the flow velocity can be computed by Eq.(4). Finally, the leakage rate L can be calculated by

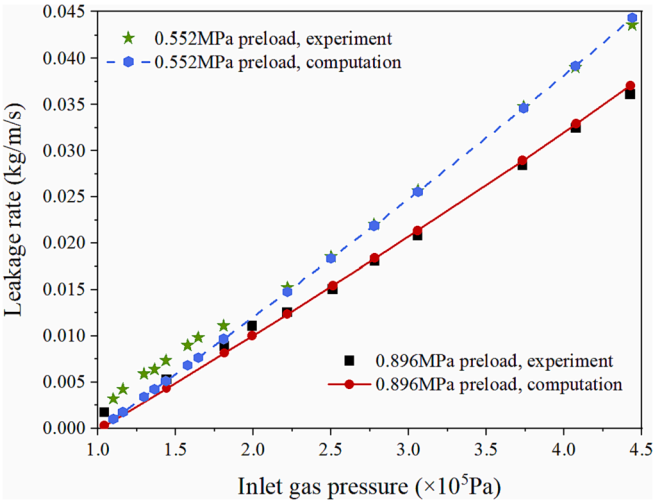

Fig. 9. Measured and computed leakage rates for M6a-1 seal strip.

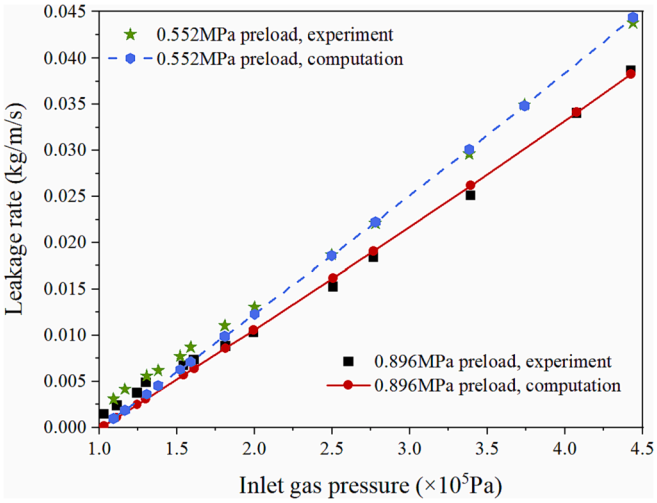

Fig. 10. Measured and computed leakage rates for M6b-1 seal strip.

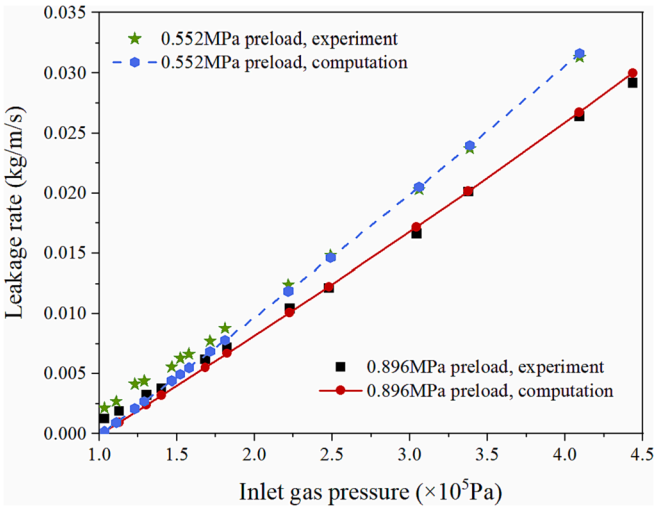

Fig. 11. Measured and computed leakage rates for M6c-1 seal strip.

integrating the velocities along the boundaries exposed to 1 atm, i.e.

$$L = \int_l \vec{v} \cdot \vec{n}\, dl \tag{62}$$

It should be noticed that in this example, L represents leakage per unit length and per second of the seal strip.

Three kinds of seals, M6a-1, M6b-1, and M6c-1 are involved in the experiments. The initial porosity Φ_0 of M6a-1, M6b-1, and M6c-1 are 0.562, 0.572, 0.515, respectively. To implement LM algorithm, the initial iterative values of three uncertain parameters a, α_0, E_0 are all set to 2.0, $6 \times 10^{-11}$and 1.28×10^7 for three seals. Through the iteration of LM algorithm, finally, one can obtain the minimum values of objective function F and their corresponding a, α_0, E_0 for three different seal strips, which are shown in Table 1. Meanwhile, for the sake of comparison, 26 groups of measured and computed leakage rates for M6a-1 seal strip are shown in Fig. 9. Similarly, those for M6b-1 and M6c-1 are shown in Fig. 10 and Fig. 11, respectively. In addition, 6 additional groups of given conditions of each seal strip are calculated by the inversion results. Their measured and computed leakage rates are shown in Table 2.

In three figures, by comparing the measured leakage rates with the computed ones, it can be concluded that parameters in Table 1 are fundamentally credible when predicting the leakage rates of three seals under high pressure differences. Meanwhile, observing the errors

Table 2
Measured and computed leakage rates of additional specified conditions.

	Preloads/ Pa	Inlet pressures/ Pa	Leakage rates/ kg•m^{-1}•s^{-1} Experiment	Computation	Errors
M6a-1	551,581	122756.2452	4.8311688E-03	2.5892085E-03	5.81 %
	551,581	150351.7427	7.9231169E-03	5.9469631E-03	5.14 %
	551,581	199905.563	1.3044156E-02	1.2055381E-02	2.61 %
	551,581	338458.8189	2.9566753E-02	2.9852199E-02	0.63 %
	896,318	167219.4449	7.6332468E-03	6.6872168E-03	2.48 %
	896,318	339516.626	2.4252468E-02	2.5117215E-02	2.12 %
M6b-1	551,581	123353.4713	4.7448156E-03	2.7204952E-03	5.32 %
	551,581	145352.6169	7.1656399E-03	5.4501733E-03	4.59 %
	551,581	221501.6257	1.5396443E-02	1.5013525E-02	1.18 %
	551,581	306126.9772	2.5757570E-02	2.5897442E-02	0.11 %
	896,318	167327.3245	7.9170696E-03	7.0731033E-03	2.48 %
	896,318	372629.0601	2.9635016E-02	3.0026511E-02	0.14 %
M6c-1	551,581	138117.2135	5.1196781E-03	3.5768396E-03	5.35 %
	551,581	164829.3684	7.5447887E-03	6.1989520E-03	4.71 %
	551,581	204645.5994	1.0598632E-02	1.0153001E-02	1.67 %
	551,581	372982.576	2.7574406E-02	2.7662515E-02	0.22 %
	896,318	121485.117	2.5149296E-03	1.6459690E-03	3.06 %
	896,318	373486.5789	2.2814004E-02	2.3419498E-02	1.27 %

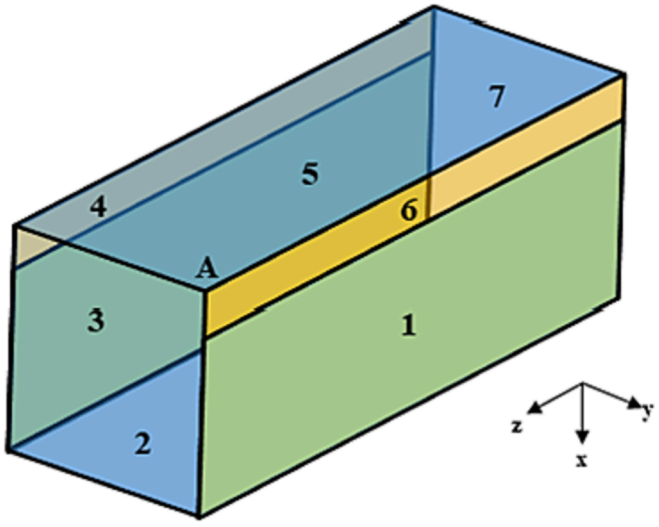

Fig. 12. Computational model of the example 2.

between the experimental values and the computational values from three figures and Table 2, it can also be found that the higher the inlet gas pressures are, the less the errors are. Regarding this phenomenon, the authors believe that there may be two reasons. The first one is that the experimental results may have some errors when the inlet gas pressures are close to 1 atm. Generally, when inlet gas pressure equals 1 atm, the leakage rate should be zero whatever the preload is. But according to the trends of the experimental results in three figures, it may

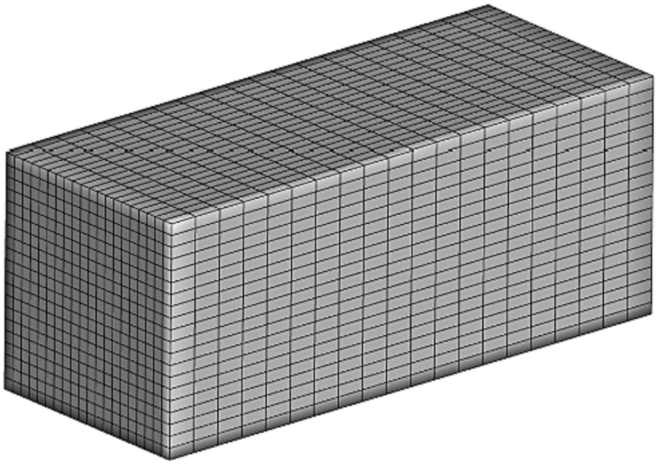

Fig. 13. 3D seal strip mesh.

not be zero. The second one is that when the gas pressure difference is close to 0, Eqs.(1) and (4) may not be suitable to describe the physical process because of the lower velocity of the fluid, similar to the views expressed in reference [10].

5. Example 2: A square cross-section 3D seal strip analysis

5.1. Steady state analysis

In the second example, a 40 mm length seal strip with 8 mm × 8 mm square section is considered. The computational model only takes half of the length because of the symmetry. As is shown in Fig. 12, the coordinate system is set up at the center of the symmetrical section square. As is shown in the figure, the upper and lower faces are divided into two parts with an area ratio of 1:4 as required by the boundary conditions, where the smaller parts are free and the larger parts are constrained by the surrounding structure in terms of their normal orientation displacements. In Fig. 12, the faces labeled 1 and 3 are fixed in the y-direction, the face labeled 2 is fixed in the x-direction, and the face labeled 7 is the symmetrical section at half of the strip length with its z-direction fixed. The face labeled 5 is exposed to 0.552 MPa uniformly distributed preload. The face labeled 6 is exposed to 800 K temperature and 409271 Pa seepage pressure, while the face labeled 4 was exposed to 300 K and 101325 Pa (1 atm). That means high temperature gases will enter from part 6 and will be leaked through part 4. Other surfaces without specified displacements or preloads are free surfaces and surfaces without specified temperatures are insulated, and surfaces without specified seepage pressures have zero leakage velocity. The heat conductivities of fiber and air are 25 W/(m·K) and 0.02 W/(m·K). Thermal expansion coefficient is 7.5 × 10^{-6} K^{-1}. Parameter a_1 is 5 × 10^{-4} K^{-1}. Other parameters and relationships are the same with those of seal M6c-1 in example 1.

To discretize this 3D computational model, 68,921 nodes and 8,000

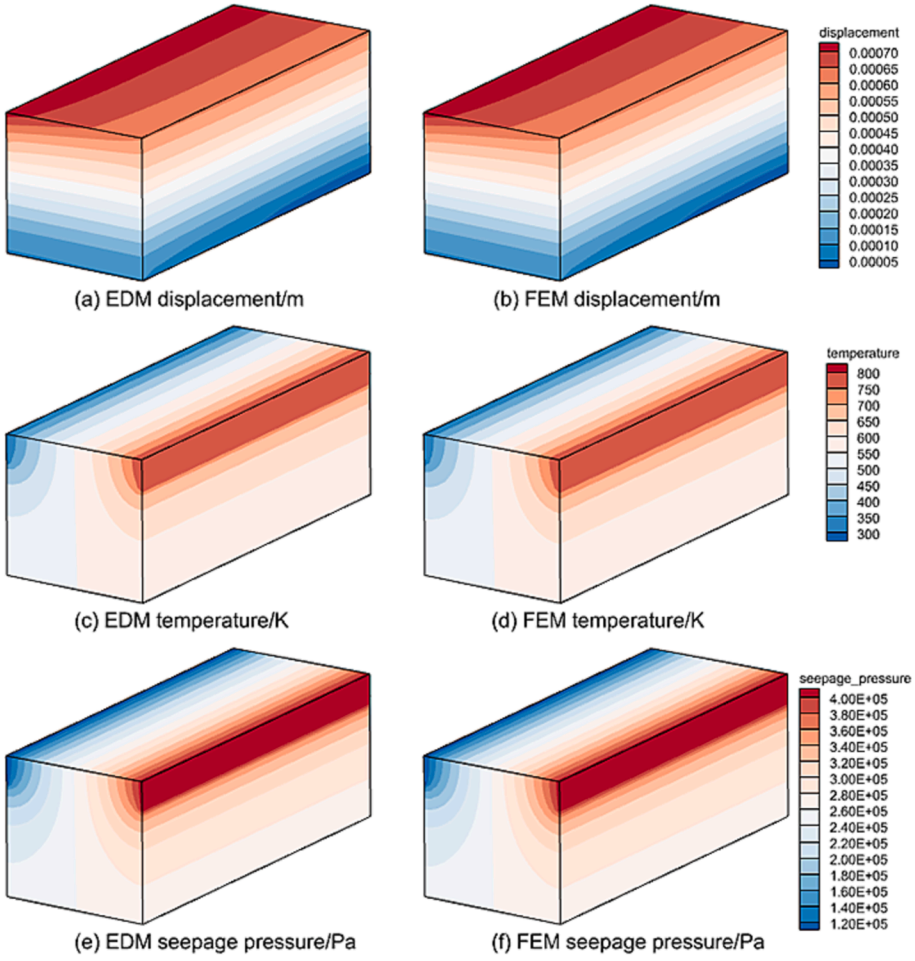

Fig. 14. The result contours of two methods.

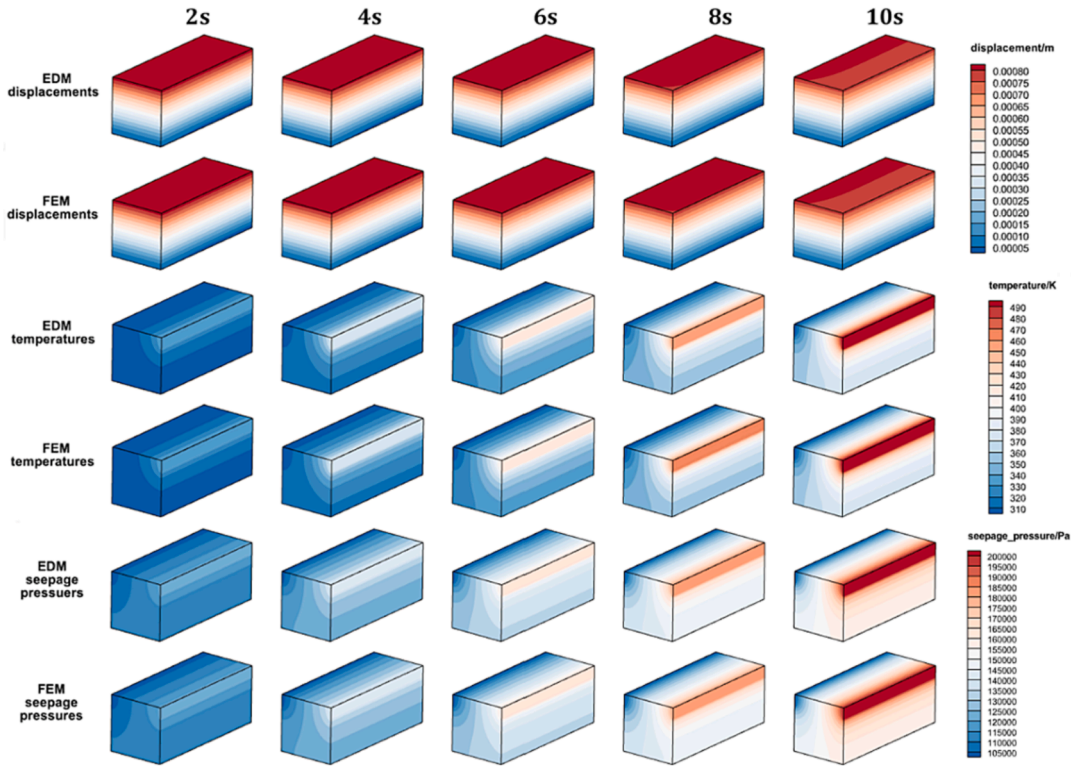

Fig. 15. The contours of EDM and FEM at 2 s, 4 s, 6 s, 8 s, and 10 s.

27-node elements are used, as are shown in Fig. 13. For the sake of comparison, the authors use two methods, EDM and conventional Galerkin FEM, to calculate this problem, for which the same mesh and the same type of elements are used. In addition, the FORTRAN programs of two methods are coded in the same framework to compare the computational time more fairly. And the linear algebraic solver is program PARDISO from Intel MKL. Besides, in steady analysis, when ∞-norm of the residual vector is less than 10^{-6}, the non-linear iteration is considered converged.

After computation, the contours of displacements, temperatures, and seepage pressures of two methods are shown in Fig. 14. Through these six contours, it can be found that the results of EDM and FEM are almost the same. However, the computational time of EDM is 1082.473 s for 14-step non-linear iteration, while that of FEM is 1221.028 s for also 14-step. This confirms that the results of EDM is reliable and EDM is more efficient than conventional Galerkin FEM when using the same mesh, which coincides with the conclusion in reference [19] (where accuracy and computational cost of EDM and FEM were detailly compared).

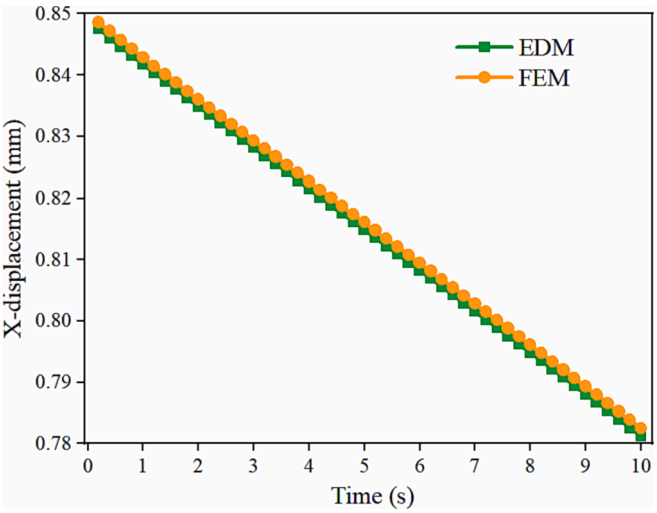

Fig. 16. The X-displacements of point A versus time of two methods.

5.2. Transient analysis

In this section, the physical changes of the seal strip are analyzed during the gradual increase of temperature and seepage pressure. The same seal strip parameters are adapted in the transient analysis. To implement transient analysis, some extra properties need to be specified. Fiber density ρ_s is 2500 kg/m^3. Specific heat of fibers and air are 840 J/(kg·K) and 1005 J/(kg·K), respectively. Fluid compressibility coefficient β_p is 9.869×10^{-6}. The thermal volume expansion coefficient of fluid β_t is -3.333×10^{-3}. The length orientation is along z-axis (i.e., x_3 direction), and the elastic modulus along the length orientation is $E_3 = 3.5 \times 10^8$ Pa. The Poisson's ratio ν_{12} is 0.22. The Poisson's ratio ν_{32} ($=\nu_{31}$) is 0.02. And the shear modulus G_{13} ($=G_{23}$) is 0.9 times elastic modulus along two radial orientations (i.e., E_1 and E_2). Time step is set to 0.2 s and the total time is 10 s. Part 2 (in Fig. 12) is exposed to $(300 + 20{\cdot}t)$ K temperature and $(101325 + 10000{\cdot}t)$ Pa seepage pressure, where t represents elapsed time. The other boundary conditions are not changed.

After calculation, the displacement, temperature, and seepage pressure contours of EDM and FEM at 2 s, 4 s, 6 s, 8 s, and 10 s are obtained and shown in Fig. 15. The X-displacements of point A (see Fig. 12) versus time of two methods are shown in Fig. 16. Through Fig. 15 and Fig. 16, it can also be found that the results of EDM and FEM are almost the same. Meanwhile, through the displacement contours and Fig. 16, it can be found that the seal strip deformation will have slight change in the opposite orientation of 0.552 MPa preload. It may be partly because of thermal expansion and partly due to the decrease of porosity caused by the increase of compression volumetric strain, which will in turn leads to an increase of the elastic modulus, finally resulting in this deformation

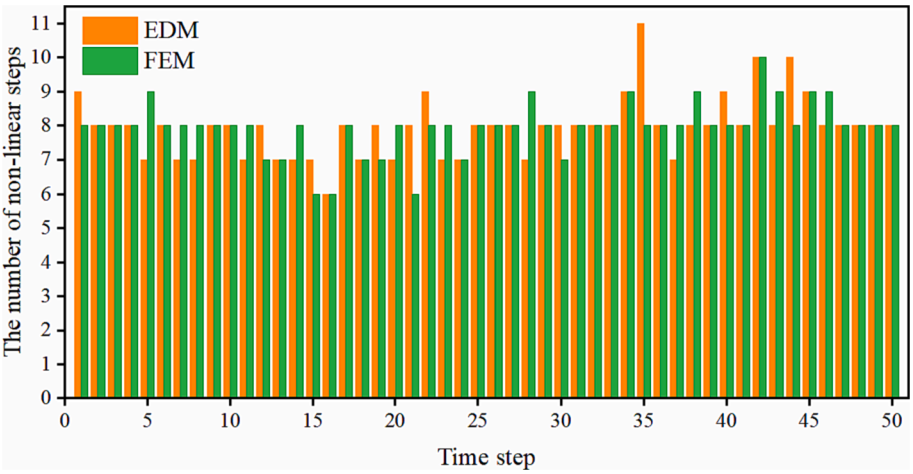

Fig. 17. The number of non-linear iterative steps for each time step of two methods.

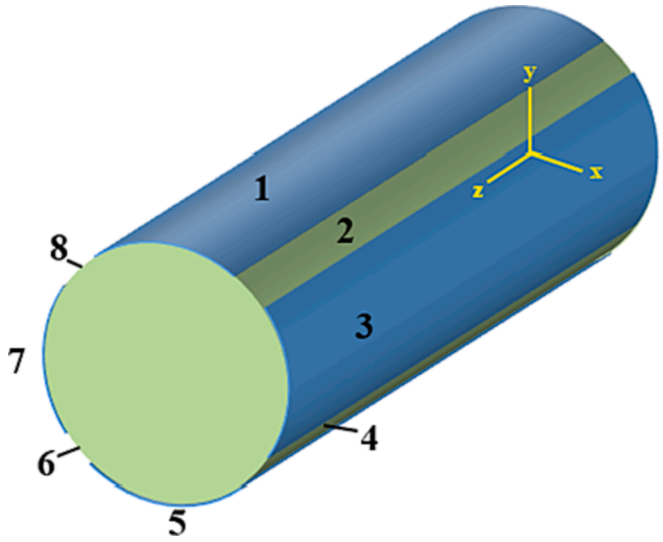

Fig. 18. Computational model of the example 2.

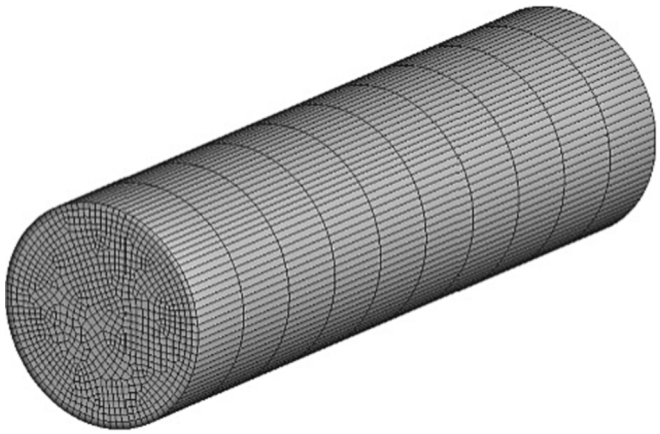

Fig. 19. 3D seal strip mesh.

against preload. In addition, the number of non-linear iterative steps for each time step of two methods are shown in Fig. 17. From Fig. 17, it can be found that they are not exactly the same. Nevertheless, the total non-linear steps for two methods both happen to be 397 steps. And the computational time of EDM is 29194.456 s, while that of FEM is 34592.271 s.

6. Example 3: A circular cross-section 3D seal strip analysis

6.1. Steady state analysis

In the third example, a seal strip with the diameter of 6 mm and length of 40 mm is considered and, also, the computational model only takes half of the length because of the symmetry. As is shown in Fig. 18, the coordinate system is set up at the center of the symmetry section circle. The seal strip is compressed from four directions, top, bottom, left, and right, and the compression size of each direction is 0.6 mm. According to the compressed areas, the surface of the seal strip is separated into 8 parts, as is shown in Fig. 18. Parts 1, 3, 5, and 7 (colored orange) are moved to plane y = 2.4 mm, x = 2.4 mm, y = -2.4 mm, and x = -2.4 mm, respectively. That means, for example, the y-displacements of the nodes on part 1 satisfy (2.4-y) mm, where y represents y-coordinates of the nodes, and the other two directions are free. The z-direction of the symmetry section is fixed, while the other two directions are free. High temperature gases will enter from part 2 and will be leaked through part 4. That means, part 2 is exposed to 800 K temperature and 409271 Pa seepage pressure, while part 4 is exposed to 300 K temperature and 101325 Pa (1 atm) seepage pressure. Other surfaces whose displacements are not assigned are free surfaces and whose temperatures are not assigned are insulated and whose seepage pressures are not assigned have zero leakage velocity.

To discretize the 3D computational model, 78,603 nodes and 9120 27-node elements are used, as shown in Fig. 19. In this example, the material parameters are the same with those of seal M6a-1 in example 1. Some other parameters like thermal expansion coefficient, heat conductivities of fiber and air are the same with the seal in example 2, except for the Poisson's ratio ν_{32} ($=\nu_{31}$) becoming 0.12.

After computation, the contours with deformations of displacements, temperatures, and seepage pressures of two methods are shown in Fig. 20. Through these six contours, it can be found that the results of EDM and FEM are almost the same. However, the computational time of EDM is 823.839 s for 10-step non-linear iteration, while that of FEM is 902.302 s for also 10-step. This confirms again for curve geometry that the results of EDM are reliable and EDM is more efficient than FEM when using the mesh.

6.2. Transient analysis

Also, in the second part, the physical changes of the circular cross-section seal strip are analyzed in the process of temperature and

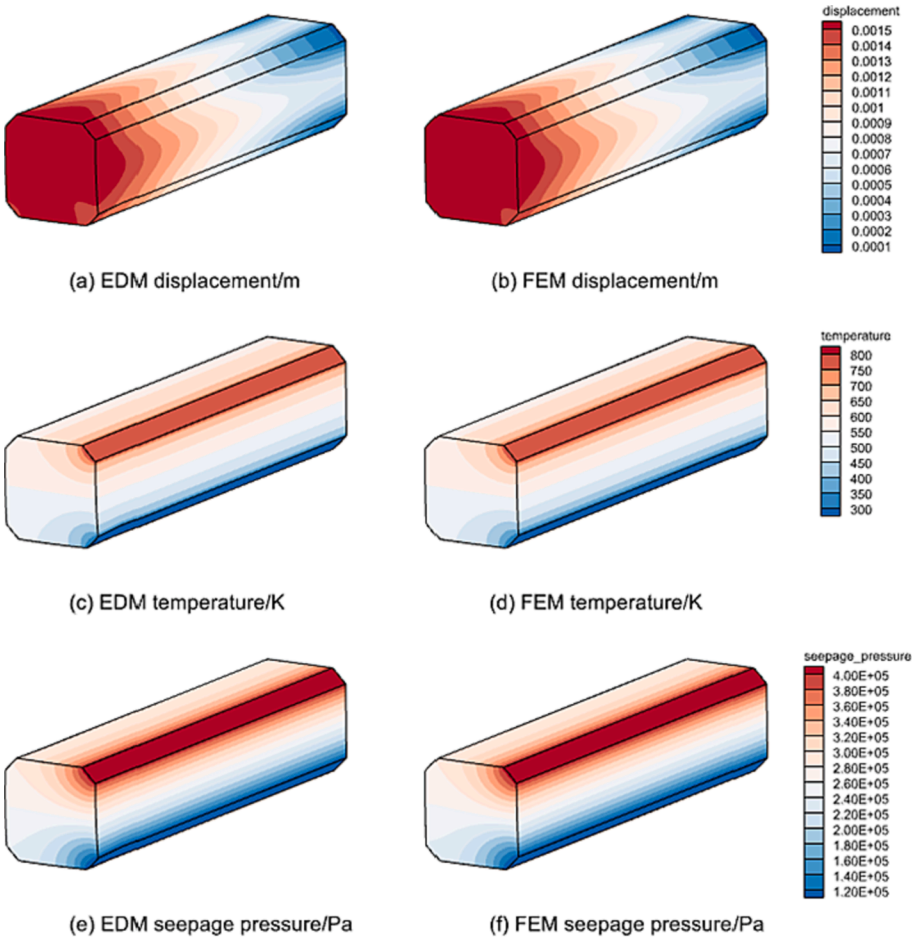

Fig. 20. The result contours with deformations.

seepage pressure gradually increasing. The same seal strip model is adapted in the transient analysis. Fiber density, specific heat of fiber and air, fluid compressibility coefficient, thermal volume expansion coefficient of fluid are the same with those in example 2. Time step is also set to 0.2 s and the total calculation time is 10 s. Part 2 (in Fig. 18) is exposed to $(300 + 20{\cdot}t)$ K temperature and $(101325 + 10000{\cdot}t)$ Pa seepage pressure. The other boundary conditions are not changed.

Through calculation, the temperature and seepage pressure contours at 2 s, 4 s, 6 s, 8 s, and 10 s are obtained and shown in Fig. 21. The results of EDM and FEM are almost the same. The number of non-linear iterations for each time step of two methods are shown in Fig. 22, which shows that numbers of non-linear iterations for each time period are not the same. The total number of non-linear iterations of EDM is 356 steps, and slightly more than FEM of 346. The computational time of EDM is 29476.199 s, while that of FEM is 32668.702 s.

7. Conclusion

In this paper, the mechanics-thermal-seepage coupled model is used to analyze the working process of the braided ceramic fiber seal strips. Elasticity, thermal, and seepage governing equations are used and some parameter assumptions are made about the relationships among porosity, elasticity modulus, temperature, permeability, and volumetric strain. Meanwhile, element differential method is employed to obtain the numerical solutions of the coupled problems.

To obtain the material-dependent parameters in the relationship formulas, the authors use the experimental leakage rates under various circumstances to implement an inverse analysis by LM algorithm. And the good agreement of experimental statistics and inversion results verify that the inversion parameters are credible. Meanwhile, the authors also conclude two possible reasons for errors between experiments and computations at low inlet gas pressure. One is that the errors may exist in the experimental measurements and the other is that different formulas may be applicable for the low velocity flow case.

Steady state analysis and transient analysis of a 3D square-section and a circular-section seal strip are given, respectively, to solve for the distributions of displacements, temperatures, and seepage pressures and those over time. All the analyses both verify that EDM can deliver almost the same results with FEM for this problem. Meanwhile, it can be found that EDM is more efficient than conventional Galerkin FEM in calculating this problem when using the same mesh and the same type of elements.

Data availability.

The raw/processed data required to reproduce these findings cannot be shared at this time as the data also forms part of an ongoing study.

CRediT authorship contribution statement

Yong-Tong Zheng: Writing – original draft, Methodology, Software, Investigation, Formal analysis, Writing – original draft, Visualization. **Xiao-Wei Gao:** Methodology, Funding acquisition, Resources, Investigation, Writing – review & editing. **Yijun Liu:** Writing – review & editing, Resources.

Declaration of Competing Interest

The authors declare that they have no known competing financial interests or personal relationships that could have appeared to influence

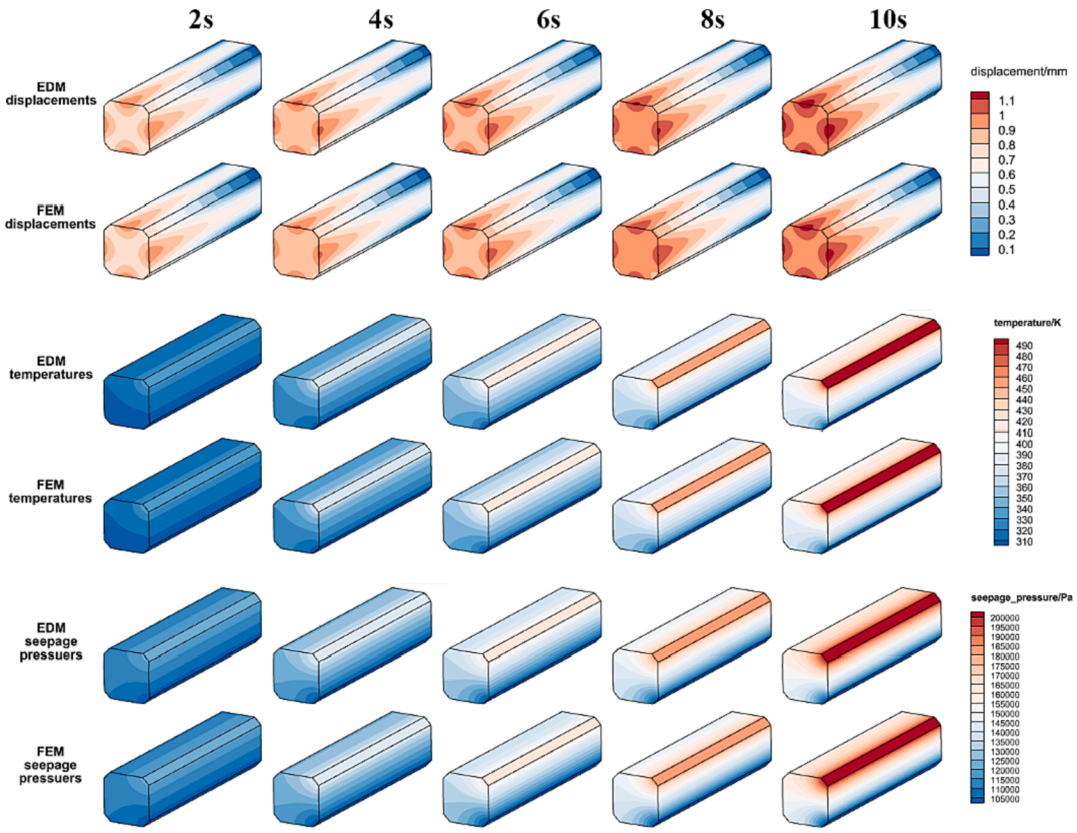

Fig. 21. The result contours at 2 s, 4 s, 6 s, 8 s, and 10 s.

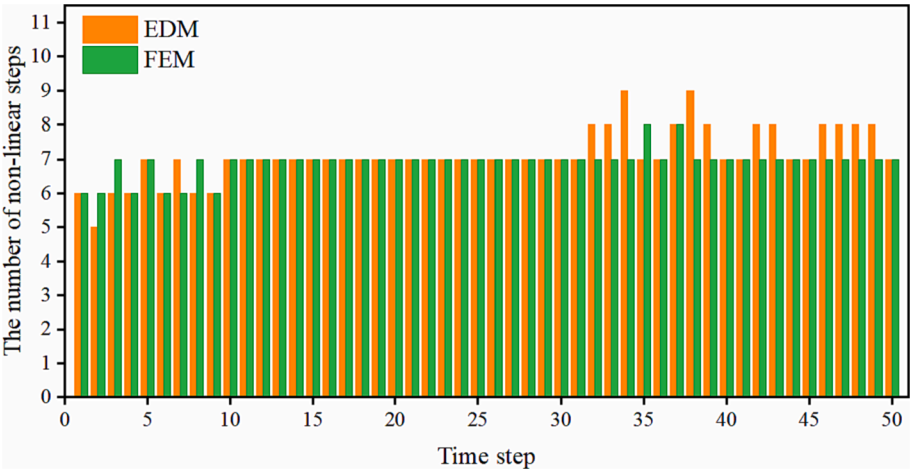

Fig. 22. Numbers of non-linear iterations for each time step of two methods.

the work reported in this paper.

Data availability

The raw/processed data required to reproduce these findings cannot be shared at this time as the data also forms part of an ongoing study.

Acknowledgment

The support of this investigation by the National Natural Science Foundation of China (Grant Nos. 12072064) is gratefully acknowledged.

References

[1] Liu Y, Wang L, Qian Z. Numerical investigation on the assistant restarting method of variable geometry for high Mach number inlet. Aerosp Sci Technol 2018;79:647–57. https://doi.org/10.1016/J.AST.2018.06.014.

[2] Dou L, Gao J, Zong Q, Ding Z. Modeling and switching control of air-breathing hypersonic vehicle with variable geometry inlet. J Franklin Inst 2018;355:6904–26. https://doi.org/10.1016/J.JFRANKLIN.2018.07.007.

[3] Qin Q, Xu J, Guo S. Aeroelastic study of the splitter plate in turbine-based combined-cycle inlet. J Aircr 2018;55:1914–28. https://doi.org/10.2514/1.C034649.

[4] Liu XW, Shi L, Liu PJ, He GQ. Investigation of a variable engine inlet with geometry combined cycle double passage. J Solid Rocket Technol 2016;39:746–50. https://doi.org/10.7673/j.issn.1006-2793.2016.06.002.

[5] Wang LH, Wang JH, Yang BW. Dynamic Seal Technology for Control Surface of Hypersonic Vehicles. Aerosp Mater Technol 2016;46:1–6. https://doi.org/10.3969/j.issn.1007-2330.2016.03.001.
[6] Ko FK, Cai Z, Mutharasan R, Steinetz BM. Development of braided rope engine seals. 39th Int. SAMPE Symp Exhib 1994.
[7] Steinetz BM, Adams ML, Bartolotta PA, Darolia R, Olsen A. High-Temperature Braided Rope Seals for Static Sealing Applications. J Propuls Power 1997;13:675–82. https://doi.org/10.2514/2.5219.
[8] Mutharasan R, Steinetz BM, Tao XM, Ko F. Development of braided rope seals for hypersonic engine applications. In: Part II: Flow modeling. 27th Jt. Propuls. Conf; 1991. https://doi.org/10.2514/6.1991-2495.
[9] Cai Z, Mutharasan R, Ko FK, Steinetz BM. Characterizing the Leakage Flow of Braided Fiber Seals. Text Res J 1994;64:1–9. https://doi.org/10.1177/004051759406400101.
[10] Cai Z, Mutharasan R, Ko FK, Steinetz BM. Development of hypersonic engine seals - Flow effects of preload and engine pressures. J Propuls Power 1994;10:884–9. https://doi.org/10.2514/3.23827.
[11] Ergun S. Fluid flow through packed columns. Chem Eng Prog 1952;48:89–94.
[12] Zienkiewicz OC, Taylor RL. The finite element method. vol. 84. sixth ed. London: ELsevier; 2005.
[13] Gao XW, Davies TG. Boundary element programming in mechanics. Cambridge, UK: Cambridge University Press; 2002.
[14] Belytschko T, Krongauz Y, Organ D, Fleming M, Krysl P. Meshless methods: An overview and recent developments. Comput Methods Appl Mech Eng 1996;139:3–47. https://doi.org/10.1016/S0045-7825(96)01078-X.
[15] Nguyen TN, Ngo TD, Nguyen-Xuan H. A novel three-variable shear deformation plate formulation: Theory and Isogeometric implementation. Comput Methods Appl Mech Eng 2017;326:376–401. https://doi.org/10.1016/J.CMA.2017.07.024.
[16] Nguyen TN, Thai CH, Luu AT, Nguyen-Xuan H, Lee J. NURBS-based postbuckling analysis of functionally graded carbon nanotube-reinforced composite shells. Comput Methods Appl Mech Eng 2019;347:983–1003. https://doi.org/10.1016/J.CMA.2019.01.011.
[17] Yang K, Jiang G-H, Li H-Y, Zhang Z, Gao X-W. Element differential method for solving transient heat conduction problems. Int J Heat Mass Transf 2018;127:1189–97. https://doi.org/10.1016/j.ijheatmasstransfer.2018.07.155.
[18] Gao X-W, Li Z-Y, Yang K, Lv J, Peng H-F, Cui M, et al. Element differential method and its application in thermal-mechanical problems. Int J Numer Methods Eng 2018;113:82–108. https://doi.org/10.1002/nme.5604.
[19] Zheng Y-T, Gao X-W, Lv J, Peng H-F. Weak-form element differential method for solving mechanics and heat conduction problems with abruptly changed boundary conditions. Int J Numer Methods Eng 2020:121. https://doi.org/10.1002/nme.6379.
[20] Gao X-W, Zheng Y-T, Fantuzzi N. Local least squares element differential method for solving heat conduction problems in composite structures. Numer Heat Transf Part B Fundam 2020;77:441–60. https://doi.org/10.1080/10407790.2020.1746584.
[21] Lv J, Shao MJ, Cui M, Gao XW. An efficient collocation approach for piezoelectric problems based on the element differential method. Compos Struct 2019:230. https://doi.org/10.1016/j.compstruct.2019.111483.
[22] Gao L-F, Gao X-W, Feng W-Z, Xu B-B. A time domain element differential method for solving electromagnetic wave scattering and radiation problems. Eng Anal Bound Elem 2022;140:338–47. https://doi.org/10.1016/j.enganabound.2022.04.025.
[23] Gao X-W, Liu H-Y, Lv J, Cui M. A novel element differential method for solid mechanical problems using isoparametric triangular and tetrahedral elements. Comput Math with Appl 2019;78:3563–85. https://doi.org/10.1016/j.camwa.2019.05.026.
[24] Lv J, Song C, Gao X-W. Element differential method for free and forced vibration analysis for solids. Int J Mech Sci 2019;151:828–41. https://doi.org/10.1016/j.ijmecsci.2018.12.032.
[25] Cui M, Xu B-B, Lv J, Gao X-W, Zhang Y. Numerical solution of multi-dimensional transient nonlinear heat conduction problems with heat sources by an extended element differential method. Int J Heat Mass Transf 2018;126:1111–9. https://doi.org/10.1016/j.ijheatmasstransfer.2018.05.100.
[26] Gao X-W, Huang S-Z, Cui M, Ruan B, Zhu Q-H, Yang K, et al. Element differential method for solving general heat conduction problems. Int J Heat Mass Transf 2017;115:882–94. https://doi.org/10.1016/j.ijheatmasstransfer.2017.08.039.
[27] Gao X-W, Liu H-Y, Xu B-B, Cui M, Lv J. Element differential method with the simplest quadrilateral and hexahedron quadratic elements for solving heat conduction problems. Numer Heat Transf Part B Fundam 2018;73:206–24. https://doi.org/10.1080/10407790.2018.1461491.
[28] Levenberg K. A method for the solution of certain non-linear problems in least squares. Q Appl Math 1944;2:164–8. https://doi.org/10.1090/qam/10666.
[29] Marquardt DW. An algorithm for least-squares estimation of non-linear parameters. J Soc Ind Appl Math 1963;2:431–41. https://doi.org/10.1137/0111030.
[30] Cui M, Zhao Y, Xu B, Gao X. A new approach for determining damping factors in Levenberg-Marquardt algorithm for solving an inverse heat conduction problem. Int J Heat Mass Transf 2017;107:747–54. https://doi.org/10.1016/j.ijheatmasstransfer.2016.11.101.
[31] Zhang B, Mei J, Cui M, Gao X, Zhang Y. A general approach for solving three-dimensional transient nonlinear inverse heat conduction problems in irregular complex structures. Int J Heat Mass Transf 2019;140:909–17. https://doi.org/10.1016/j.ijheatmasstransfer.2019.06.049.
[32] Zheng Y-T, Gao X-W, Liu S, Man Y-J, Yang K. Multi-physics coupling analysis of rope-sealed structures with braided ceramic fibres by element differential method. Int J Comput Methods Exp Meas 2021:9. https://doi.org/10.2495/CMEM-V9-N2-153-164.
[33] Noorishad J, Tsang C-F. Coupled thermohydroelasticity phenomena in variably saturated fractured porous rocks - formulation and numerical solution. Dev Geotech Eng 1996;79:93–134. https://doi.org/10.1016/S0165-1250(96)80023-X.
[34] Sheng JC. Fully Coupled Thermo-Hydro-Mechanical Model Of Saturated Porous Media And Numerical Modelling. Chinese J Rock Mech Eng 2006;25:3028–33. https://doi.org/10.3321/j.issn:1000-6915.2006.z1.066.